Chronology of Upper Paleolithic human activities recorded in a stalagmite at Points Cave (Aiguèze, Gard, France)

Maïlys Richard, Edwige Pons-Branchu, Hélène Valladas, Michael Toffolo, Stéphan Dubernet, Arnaud Dapoigny, Jean-pascal Dumoulin, Pierre-Antoine Beauvais, Julien Monney

Chronology of Upper Palaeolithic human activities recorded in a stalagmite at Points Cave (Aiguèze, Gard, France)

Maïlys Richard[1, 2]*, Edwige Pons-Branchu[1], Hélène Valladas[1], Michael B. Toffolo[2,3], Stéphan Dubernet[2], Arnaud Dapoigny[1], Jean-Pascal Dumoulin[4], Pierre-Antoine Beauvais[5], Julien Monney[6]

[1] Laboratoire des Sciences du Climat et de l'Environnement, GEOTRAC-LSCE/IPSL, UMR 8212, CEA-CNRS-UVSQ, Université Paris-Saclay, Gif-sur-Yvette, France

[2] Archéosciences Bordeaux, UMR 6034 CNRS, Université Bordeaux Montaigne, Maison de l'Archéologie, Pessac, France.

[3] Department of Early Prehistory and Quaternary Ecology, University of Tübingen, Tübingen, Germany

[3] Geochronology and Geology Program, Centro Nacional de Investigación sobre la Evolución Humana (CENIEH), Paseo Sierra de Atapuerca 3, Burgos, Spain.

[4] Laboratoire de Mesure du Carbone 14 (LMC14), LSCE/IPSL, CEA-CNRS-UVSQ, Université Paris-Saclay, Gif-sur-Yvette, France.

[5] Laboratoire TRACES, UMR 5608, Université Toulouse Jean Jaurès, Maison de la Recherche, 5, allées Antonio Machado, Toulouse, France.

[6] Laboratoire EDYTEM, Université Savoie Mont Blanc, Bd de la mer Caspienne, Le Bourget du Lac, France.

*Corresponding author: mailys.richard@u-bordeaux-montaigne.fr

Abstract

In this article, we propose an approach to reconstruct the timing of human activity at Points Cave, an Upper Palaeolithic rock art site located in the middle of the Ardèche River gorge (Rhône valley, France), based on the dating and characterisation of a stalagmite containing soot.

Points Cave ("Grotte aux Points" in French), also called the "little sister of Chauvet Cave", is famous for its parietal art including a series of dots made of palm prints. A large number of stalagmites formed in the cave during the last 500 ka. However, quarrying of the cave floors during historic times led to the partial destruction of the sedimentary deposits, and many of the stalagmites were found lying on the floor. In particular, one of them (STM-18-04) showed the presence of at least four dark layers in cross-section, which appeared as possible remnants of fire-related activities in the cave.

Despite being present at the same site, no other specific link between STM-18-04 and the rock art has been documented. This stalagmite, however, allows us to identify phases of human presence, located at the cave entrance. In order to do so, we performed a series of analyses to determine its period of growth and the nature of the dark layers it contains. Scanning electron microscopy and Raman micro-spectroscopy confirmed that the dark layers include soot, and U-series dating indicated that the fire events occurred respectively around 14,200-14,100 and 12,500 years ago, in agreement with the radiocarbon ages of charcoal specimens recovered from the excavation areas nearby. We thus highlighted phases of human activity at the site during the Upper Magdalenian and/or beginning of the Epipalaeolithic. By comparing our results with the regional palaeoclimatic record, the soot layers trapped in the stalagmite appear to be synchronous with two cold periods, likely the Older Dryas, and the Younger Dryas.

Keywords: Stalagmite; Soot; Upper Magdalenian; Chronology; U-series; Radiocarbon; Vibrational spectroscopy; Scanning electron microscopy.

1. Introduction

Establishing the chronology of human and animal activities in Palaeolithic rock art sites in relation to natural phenomena (climate change, geological and environmental events) is a key issue in rock art research. Following the discovery of Chauvet Cave in 1994 and the publication of the radiocarbon ages obtained on the paintings (starting from ca. 36,000 years cal. BP, Clottes *et al.*, 1995), there has been a major effort to unravel the chronology of events that took place in the Palaeolithic rock art sites of south-eastern France (Valladas, et al., 2001, 2017; Genty et al., 2004; Ambert et al., 2005; Cuzange, et al., 2007; Azéma et al., 2012; Sadier et al., 2012; Quiles, et al., 2013; Monney et al., 2014; Guibert et al., 2015; Quiles, et al., 2016; Monney & Jaillet, 2019). There is increased interest in understanding the climatic and environmental conditions at the time of human presence at the entrance and/or in the deepest parts of rock art caves during the Upper Palaeolithic, a period that broadly ranges from ca. 50 to 12 ka. In this regard, the analysis and dating of speleothems has proved an essential source of information, especially in the Ardèche River Gorge (Bourdin, et al., 2011; Genty et al., 2004).

Uranium-series (^{230}Th/U) dating is extensively used to date calcium carbonate deposits, in particular cave speleothems (Ivanovich and Harmon, 1992; Richards and Dorale, 2003). In stalagmites, U-series dating can be combined with palaeoclimatic and palaeoenvironmental analyses, including stable isotopes and trace elements. In addition to geochemical information, speleothems may also contain remnants of anthropic activities such as traces of fire, or use of manganese oxides (e.g., Genty, et al., 1997; Vandevelde, et al., 2017; Pons-Branchu et al., 2022).

However, applications are successful on well preserved samples, i.e., closed systems, and are limited in the case that U is remobilised due to diagenetic processes (dissolution, recrystallisation), which may distort the ages obtained. This is particularly restrictive when dating thin speleothems ("crusts") covering rock art (e.g., Aubert et al., 2014; Hoffmann et al., 2016; Pike et al., 2012), thus highlighting the importance of having a clear stratigraphic control, independent dating methods (e.g., radiocarbon) and archaeological context (Pons-Branchu et al., 2014a; 2022).

Here, we combined U-series and radiocarbon (^{14}C) dating on calcite samples and material characterisation of dark particles trapped in a stalagmite collected on the floor of Points cave (STM-18-04), a rock art site located in the Ardèche River Gorge in France (Figure 1). Our study aimed at connecting chronological data obtained in STM-18-04 with the remnants of fire activities trapped in this stalagmite. These data were compared with the ^{14}C ages obtained on charcoals collected from the stratigraphic context to reconstruct the timing of human activities at the entrance of the cave.

2. Materials and Methods

2.1. Site description and sampling

Points Cave is a Palaeolithic rock art cave located in the central part of the Ardèche River Gorge (Aiguèze, Gard, France, Figure 1a). Since 2011, it has been subject to interdisciplinary research as part of the "Datation Grottes Ornées" ("Cave Art Dating") project, coordinated by one of us (Monney, 2018a). The cave is a 110 m-long corridor (Figure 1c). It was successively occupied by cave bears during Marine Isotopic Stage 3 (MIS 3, ca. 57-29 ka, Lisiecki and Raymo, 2005) and modern humans, at least, since the Gravettian (since ca. 32,000 cal BP).

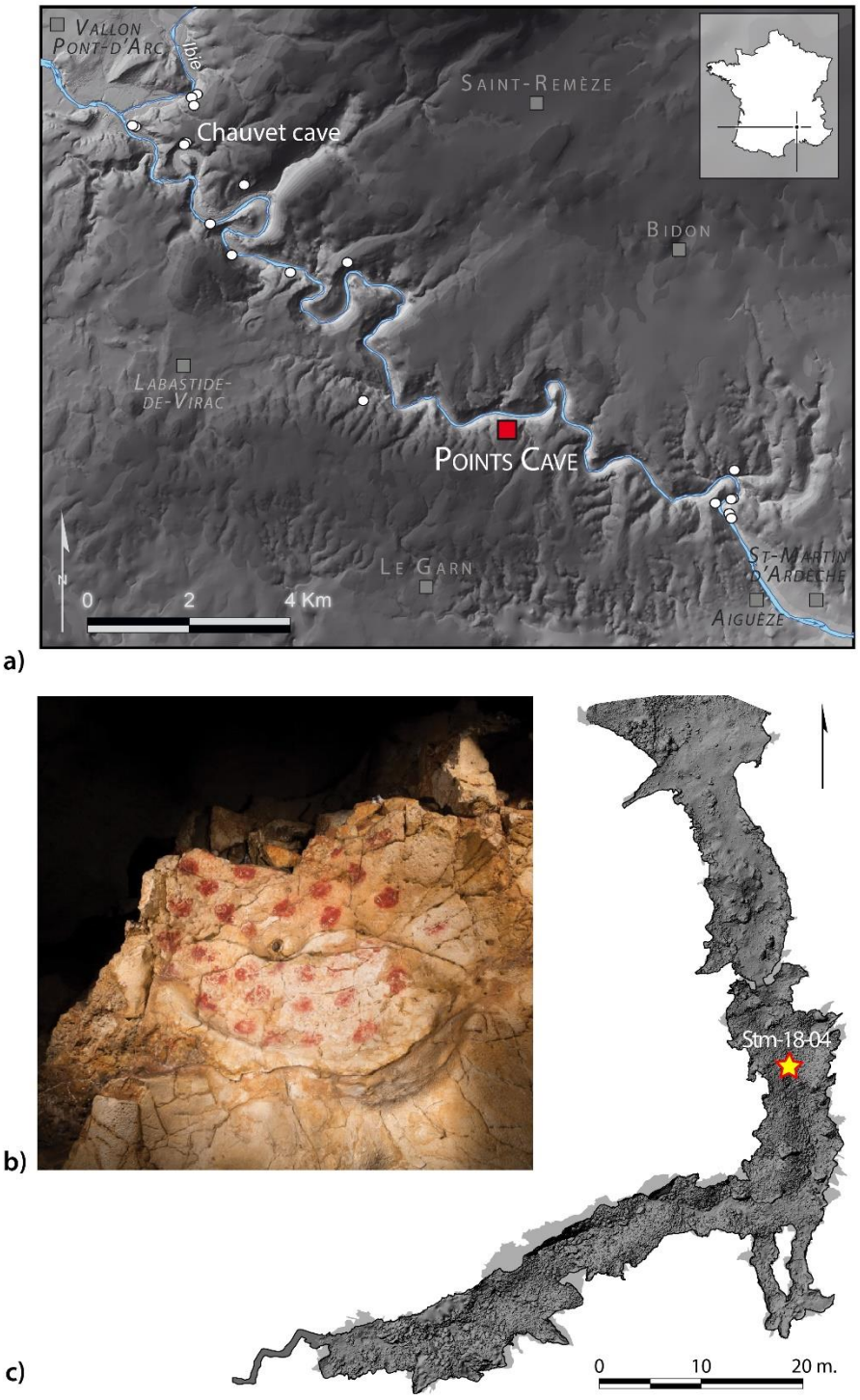

Figure 1. Location of Points Cave in the Ardèche Gorge (a), an example of palm prints produced by pressing pigment-covered palms onto the rock (b) and map of the cave with location of stalagmite STM-18-04 (c).

The rock art, which was discovered in 1993 (Brunel et al., 2008, 2018), is concentrated in an area located in the total darkness zone around 75 m from the entrance. It includes 72 red drawings and paintings, including five animal figures (three ibexes, one horse, one bison), five indeterminate tracings, two bilobed signs, one open-angle sign and 59 palm prints produced by pressing pigment-covered palms onto the rock (Figure 1b, Monney, 2018b). The rock art shows a high colorimetric homogeneity (Lafon-Pham et al., 2022) and is attributed to a single painting phase (Monney, 2018b). Its closest iconographic equivalent is to be found in the entrance sectors of Chauvet Cave, where we also find bilobed signs and palm prints clusters accompanied by small line drawings of animals (Baffier and Feruglio, 1998; Chauvet et al., 1995; Gély, 2005).

Material uncovered in SU (Stratigraphic Unit) 1 during archaeological excavations at Points Cave entrance comprises flint, charcoal, faunal remains and colouring material. The preliminary typo-technological analysis of the lithic material revealed the presence of a Noailles burin, micrograveттes, probable fragments of unifacial points, covering retouch, etc. (Boccaccio, 2018), indicating that humans visited the cave, at least during the Gravettian (ca. 32,000-26,000 cal BP) and Solutrean (ca. 26,000-21,000 cal BP) and possibly up until the Epipalaeolithic (ca. 14,000-12,000 cal BP). During historic times, the floors and sedimentary deposits of Points Cave were affected by extensive quarrying activities that led to the breakage and/or unearthing of speleothems. Archaeological surveys identified 21 stalagmites and one stalactite scattered on the floors and/or embedded in cave sediments (Figure 2).

We focused our study on one of the stalagmites, PTS-STM-18-04, whose cross-section revealed a series of dark layers interbedded with calcite (Figure 3). This stalagmite was found in the penumbra zone, 38 m away from the entrance. Following F. Rouzaud (1978), the penumbra zone is described as an area with indirect natural lighting where it is possible to move around

without the aid of artificial lighting (grease lamp, torch, etc.). Unlike other speleothems attesting to ancient flood periods inside Points Cave up to the beginning of MIS7, ca. 241 ka (Genuite et al., 2022), STM-18-04 did not show any erosion marks indicative of transport processes, nor traces of burial processes (no red sandy sediments on its outer surface). On the contrary, although found lying on the floor and disconnected from its dripping area, STM-18-04 was found intact. Moreover, remains of the sediment on which it had precipitated were still trapped under its base. Similar sediments were observed under the remnants of a broken, albeit *in situ*, stalagmitic floor located about 3 m away from STM-18-04, suggesting that the stalagmite may have been initially in the continuity of the flowstone and that it would have precipitated close to its finding place (Figure 2).

Figure 2. Location of STM-18-04 when found (1), context and floor state at Points Cave (2).

In cross-section, STM-18-04 showed a series of dark layers (Figure 3). Two of them, separated by a few millimetres, are located at the base of the stalagmite. A third layer is located less than a centimetre below the top of the stalagmite. A detailed examination of the latter showed that it resulted from the concatenation of at least two different dark horizons. The other dark traces, visible for example at the top of STM-18-04, are too diffuse to attest the presence of any other layer.

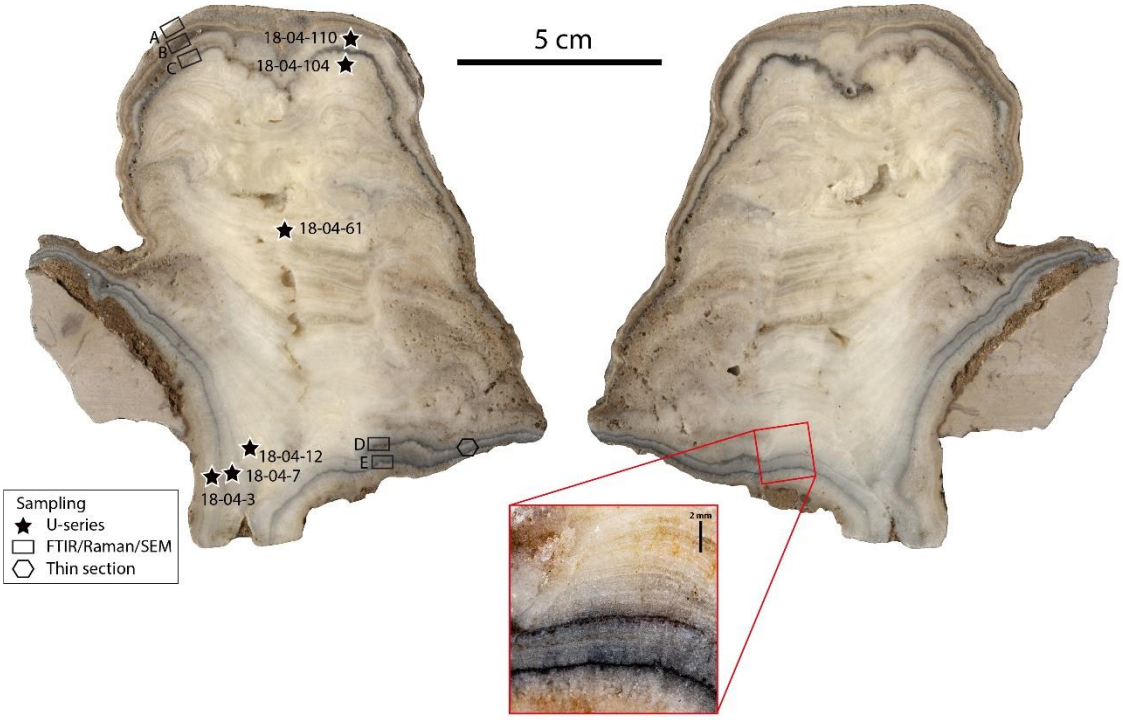

Figure 3. The STM-18-04 speleothem and location of the sampling for U-series, vibrational spectroscopy and optical microscopy. U-series samples were taken from the base to the top of the speleothem: the number after 18-04 refers to the sample depth (in mm).

These dark layers were observed using stereomicroscopy and characterised using Raman micro-spectroscopy, scanning electron microscopy (SEM), and thin section petrography (Figure 3). Six samples were also collected for U-series analyses to reconstruct the timing of

147 formation of the concretion, including the fire events (Figure 3). The crystalline phase of the
148 samples was determined using Fourier transform infrared (FTIR) spectroscopy. Radiocarbon
149 analyses were also performed on calcite and on charcoals from the immediate archaeological
150 context (stratified deposits).
151
152 **2.2. Chronology**
153 **Uranium-series dating and modelling**
154 U-series dating is based on the radioactive decay of ^{234}U in ^{230}Th within the ^{238}U decay chain.
155 Uranium being soluble in water, it is incorporated to the calcite during the precipitation of the
156 crystal. Thorium being insoluble, it is assumed that the ^{230}Th content measured today is the
157 product of the parent, ^{234}U. However, contamination of exogenous Th is common and needs to
158 be checked in order to assess the reliability of the age results. To do so, ^{232}Th, which does not
159 belong to the ^{238}U decay chain, but has the same chemical behaviour than ^{230}Th, is measured, and
160 the $^{230}Th/^{232}Th$ used to assess the level of contamination and to correct the ages (see for example
161 Hellstrom, 2006). The measurement of U and Th isotopes using mass spectrometry allows
162 calculating ages for samples up to ca. 600 ka. Six samples were extracted from STM-18-04 using
163 a dentist drill at the EDYTEM laboratory (Le-Bourget-du-Lac, France) (Figure 3). U-series
164 analyses were conducted at the Laboratory of Science of Climate and Environment (LSCE, Gif-
165 sur-Yvette, France) using the chemical procedure for separation and purification of uranium and
166 thorium isotopes described in Pons-Branchu et al. (2014b). Samples (100-200 mg) were spiked
167 with a ^{236}U-^{229}Th solution and the U and Th fractions were extracted using U-TEVA resin
168 (Eichrom®). Uranium and Thorium fractions were then recombined for measurements on a
169 Multi-Collector Inductively Coupled Plasma Mass Spectrometer (MC-ICP-MS Thermo Neptune

Plus), fitted with a jet interface and an Aridus II desolvating system. ^{238}U, ^{235}U, ^{236}U, and ^{229}Th were measured on Faraday cups, and ^{230}Th and ^{234}U on ion counting following Pons-Branchu et al. (2014b). The ages obtained were modelled using stratigraphic and coevality constraints (STRUT, Roy-Barman and Pons-Branchu, 2016). An age-depth model was then computed from corrected U-series ages and depth measurements using MOD-AGE (Hercman and Pawlak, 2012).

Radiocarbon analysis of calcite

Aliquots (ca. 10 mg) of the samples collected for U-series analyses were used for radiocarbon (^{14}C) dating at Laboratoire de Mesure du Carbone 14 (LMC14, Gif-sur-Yvette, France). $CaCO_3$ samples were cleaned according to the procedure of Dumoulin et al. (2017). The samples were then hydrolyzed in CO_2 with pure ortho-phosphoric acid (H_3PO_4) and converted to graphite prior to being measured following the standard protocols at the ARTEMIS AMS facility, LMC14 laboratory (Moreau et al., 2013; Moreau et al., 2020). The ^{14}C measurements were corrected for isotopic fractionation according to the ^{13}C values measured at the Artemis facility, following international recommendations (Mook and van der Plicht, 1999).

Radiocarbon analysis on charcoals

For comparative purposes, ^{14}C dating was also performed on five charcoals taken from the upper part of the stratigraphic sequences of the archaeological excavations previously carried out at the cave entrance. One of these charcoals (Charb-1223) comes from the natural stratigraphy visible in the background in Figure 2. It was collected at the interface between the stalagmitic floor and SU 1, in a stratigraphic position very similar to that of the two black horizons at the base of

193 STM-18-04. Two of the charcoal samples (Charb-1521 and 1525) were prepared in the "Centre
194 de Datation par le Radiocarbone" (CDRC) in Lyon (France) and sent in gas form to the
195 Laboratoire de Mesure du Carbone 14 (LMC14) in Saclay. The chemical pretreatment and the
196 combustion to produce the CO_2 of the three other charcoals (Charb-1140, 1223 and 1548) were
197 done at the LMC14 according to the protocol described in Dumoulin et al. (2017). All the
198 samples were converted to graphite and were measured at the ARTEMIS facilities. The ^{14}C ages
199 were then calibrated using Oxcal 4.4 (Bronk-Ramsey, 2001) and the IntCal20 calibration curve
200 (Reimer et al. 2020). Note that there was not enough material to perform analyses directly on the
201 black horizons.
202
203 **Stereomicroscopy and thin section petrography**
204 All speleothem fragments (A, B, C, D, and E, Figure 3) were analysed using a Leica
205 stereomicroscope at different magnifications (up to 10x) to identify regions of interest for
206 scanning electron microscopy and Raman micro-spectroscopy. One fragment of the speleothem
207 was mounted on a glass slide and polished to a thickness of 30 µm to obtain a thin section. The
208 thin section was analysed using a Leica DM2500 P polarising microscope at different
209 magnifications (25x, 50x, 100x, 200x, 400x).
210
211 **Scanning electron microscopy (SEM)**
212 Fragment D (Figure 3) was selected for SEM to determine the nature of the black particles
213 embedded in the dark layer. The sample was analysed using a JEOL JSM-IT500HR
214 InTouchScope™ at 5 kV and various working distances using a backscattered electron detector
215 for electronic mean density images and a secondary electron detector for topographic images.

Fourier transform infrared spectroscopy (FTIR)

Fragments of speleothems (*n*=6) were analysed using FTIR to determine their composition (Figure 3). In addition, two of the fragments were dissolved in 1M HCl to analyse their insoluble fraction. Samples were powdered in an agate mortar and pestle and about 5 mg of each were mixed with 40 mg of KBr and pressed into 7-mm pellets using a hand press. Infrared spectra were collected in transmission mode in 32 scans within the 4000-400 cm^{-1} spectral range using a Bruker Alpha spectrometer operated via OPUS 7.2. Spectra were analysed using OMNIC 9.6 and Macros Basic 8.0, and phase identification was based on standard literature (Farmer, 1974; van der Marel and Beutelspacher, 1976) and on the infrared spectra library of the Kimmel Center for Archaeological Science (https://centers.weizmann.ac.il/kimmel-arch/infrared-spectra-library). The degree of atomic order of calcium carbonate crystals was determined following the methods of Regev et al. (2010) and Poduska et al. (2011).

Raman micro-spectroscopy (µRaman)

Fragments of speleothems (n=3, #B, D, and E, see Figure 3) were analysed using Raman spectroscopy with a Renishaw micro-spectrometer type RM2000 coupled to a LEICA type DMLM microscope equipped with a x50 large numerical aperture objective and a 633 nm laser. Under 1-2 µm laser spot radius and the chosen optical set, the spatial resolution can be estimated to be around 3 µm along the Z depth optical axis and 2x2 $µm^2$ at the XY perpendicular matter surface. All the spectra were acquired with a grating blazed at 1200 gr/mm and a 50 µm spectrometer entrance slit, ensuring a high spectral resolution. The acquisitions are a fixed combination between a laser power attenuation and time per point, systematically adapted so that

the most intense spectral component neither exceeds the detector saturation (approximately 120,000 cts) nor damages the matter under the laser spot. Each spectrum is obtained by a summation of several consecutive acquisitions. Experimental data were processed with WIRE v1.3 Renishaw software for polynomial function background removal and curve fitting deconvolution of Raman spectral components.

The archaeological samples were compared with modern reference material including charcoal, burnt carbon fibre, and pencil graphite.

3. Results

3.1. Characterisation

FTIR shows that all the speleothem fragments are composed of calcite, as indicated by the absorption bands at 1420 (ν_3), 875 (ν_2), and 713 cm^{-1} (ν_4) (Figure 4). Despite being the product of a long geological process, calcite crystals show a poor degree of atomic order, similar to the experimental ash and archaeological lime plaster reported by Regev et al. (2010), based on the intensity of the ν_2 and ν_4 absorptions normalised to the intensity of the ν_3 absorption (Table 1). This phenomenon has already been observed in speleothems and is caused by large lattice strain in calcite crystals (Xu et al., 2015). These structural defects may be caused by porosity, inclusions, crystallite size, or morphology, which vary considerably in cave settings. Inclusions were indeed identified in thin section (Figure 5). The insoluble fractions include mainly clay minerals of the kaolinite and smectite groups (absorptions at 3697, 3622, 1037, and 521 cm^{-1}) and quartz (1080, 797, 779, 695, and 468 cm^{-1}), whereas organics related to soot were not observed, presumably because of their low concentration (Figure 4).

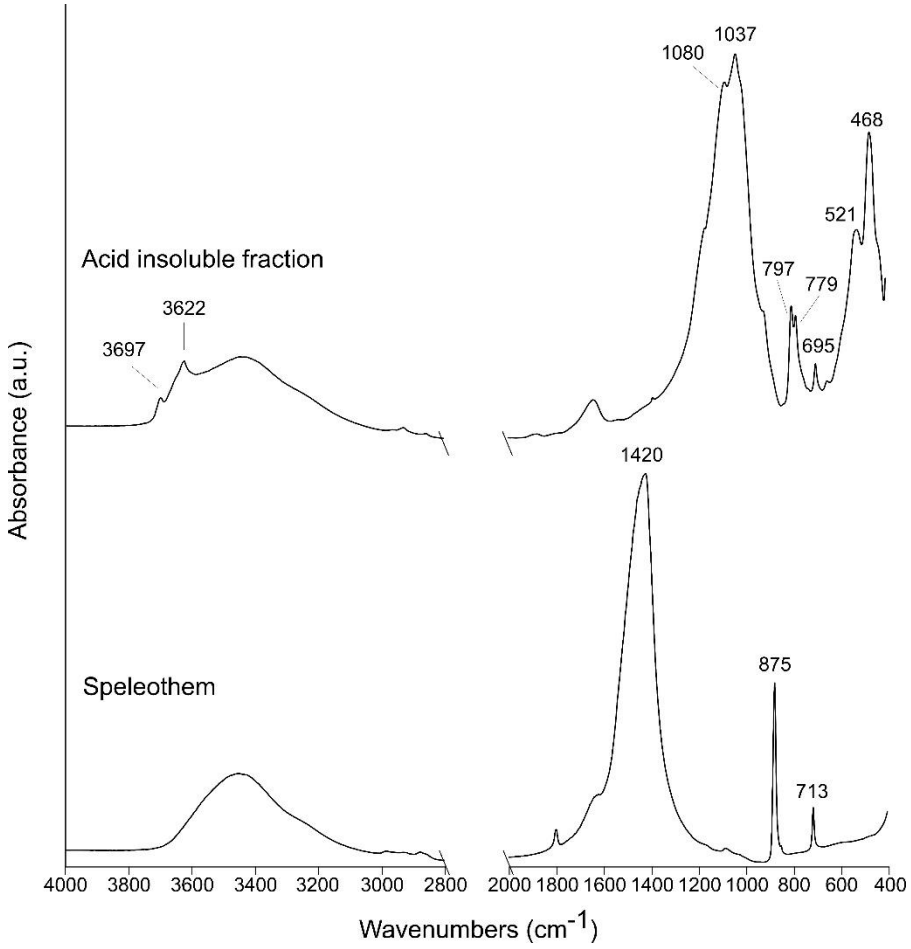

Figure 4. Representative FTIR spectra from sample D.

Sample number	**ν2**	**ν4**
STM18-04A	424	110
STM18-04B	469	120
STM18-04B+C	435	106
STM18-04C	438	98
STM18-04D	452	108
STM18-04E	456	117

Tab. 1. Intensity of the ν2 and ν4 infrared absorptions of calcite normalised to the intensity of the ν3 absorption.

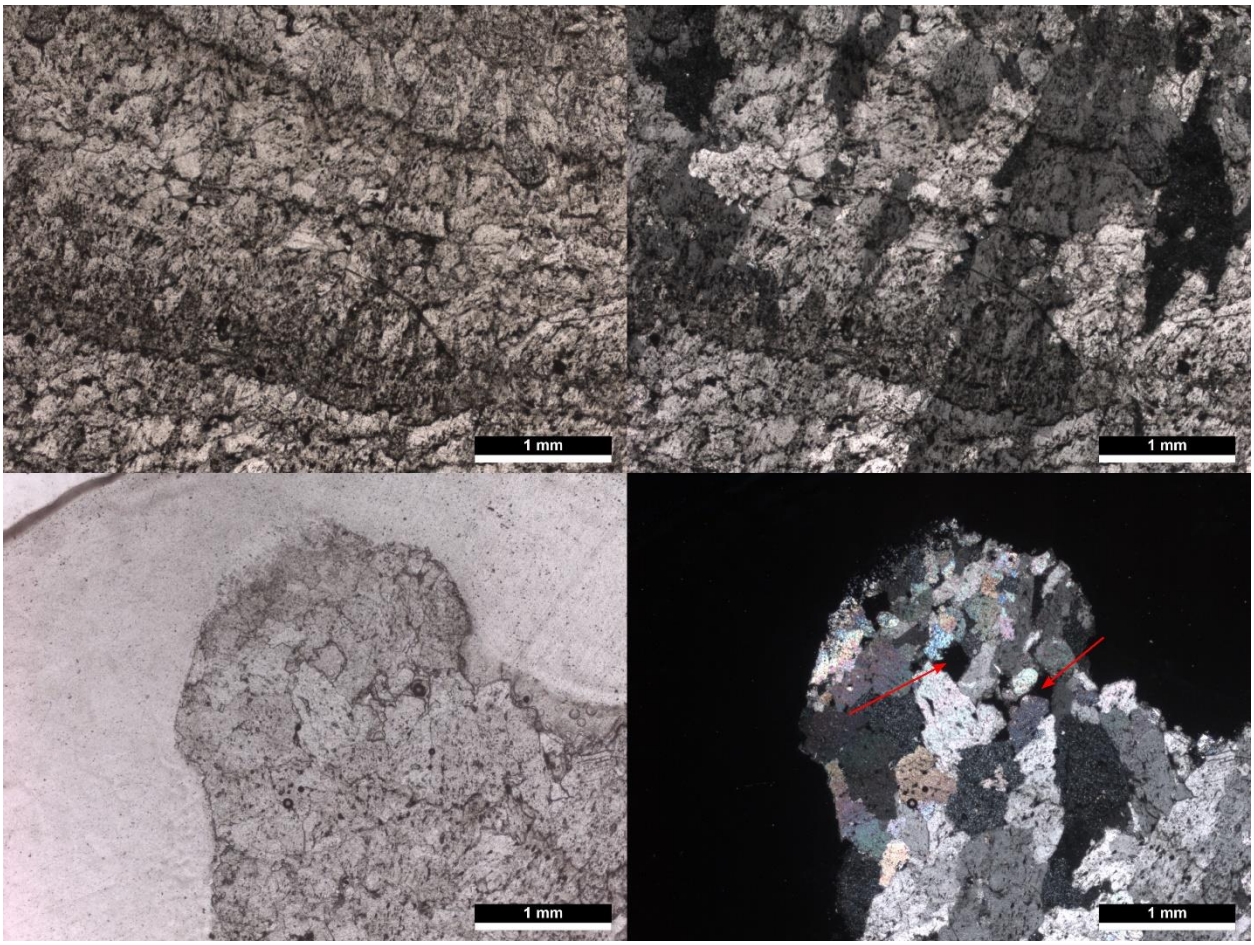

Figure 5. Photomicrographs of one of the speleothem fragments (thin section in Figure 3). Top row shows calcite layers in plane polarized light (left) and cross polarized light (right). The black spots are inclusions. Bottom row shows the outer portion of the fragment in plane polarized light (left) and cross polarized light (right). Red arrows indicate porosity.

Dark particles identified by stereomicroscopy (Figure 6) were analysed using SEM and µRaman to determine their structure and composition. Fragment D exhibits a large black particle embedded within the dark layer, which is characterised by a regular structure typical of wood anatomy, as observed in SEM (Figure 6.d). µRaman revealed that this dark particle, like many others measuring a few microns across, shows two groups of peaks: the first ranges from 1000 to

1800 cm^{-1}, the second between 2200 and 3400 cm^{-1} with an intensity ratio of 1/4 to 1/5 compared to the previous group of peaks (Figure 7, Table 2). The trapped black compound has the same Raman spectral components as burned pine charcoal rather than other carbon compounds (Figure 7). The positions and height ratios of the maxima around 1350 cm^{-1} called D band and around 1600 cm^{-1} called G band can be used as thermometric indicators (Theurer et al., 2021; Deldicque et al. 2023). The spectral curve-fitting of the STM18-04 main black inclusion is reported in SOM Table S1 for further developments.

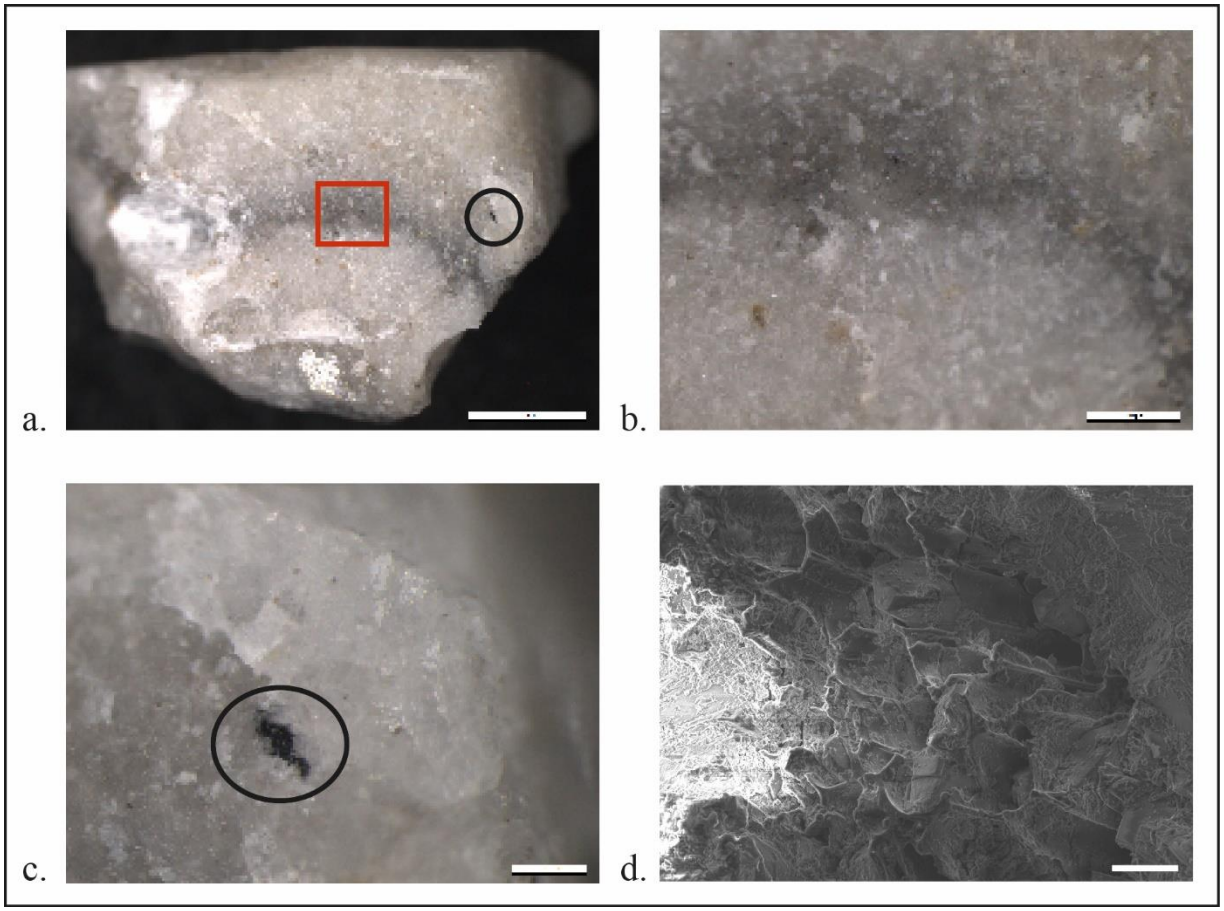

Figure 6. Stereomicroscopy (a, b, c) and SEM (d) images of fragment D. Scales are 2 mm (a), 800 µm (b), 200 µm (c) and 10 µm (d). The SEM image shows the black particle highlighted with circles in a and c. The red rectangle shows the location of image 2.

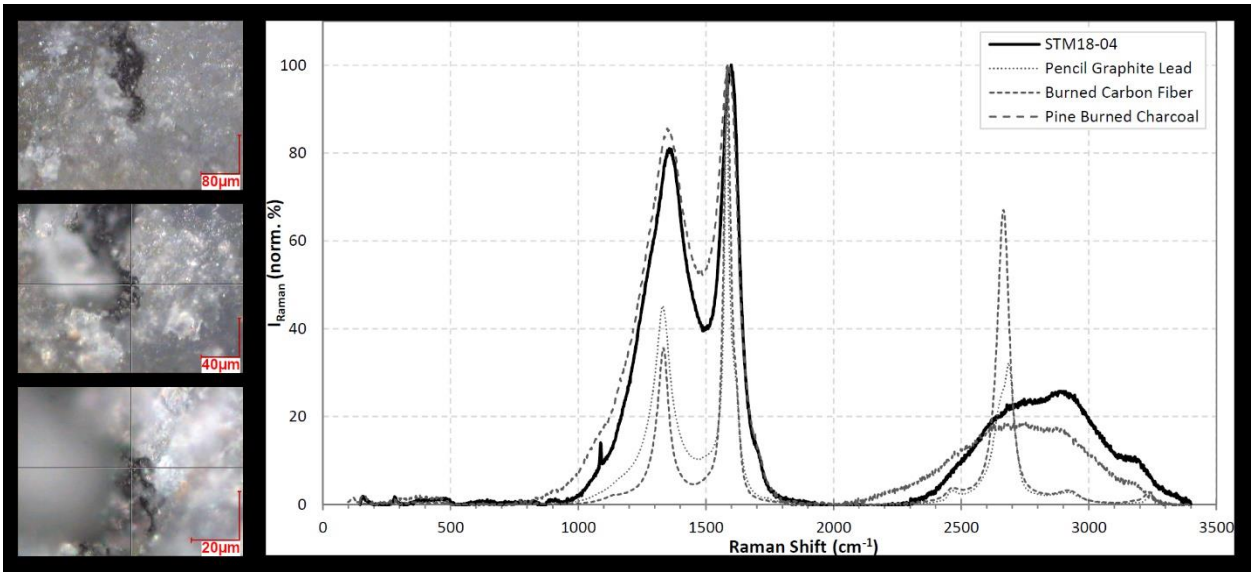

Figure 7. Photomicrographs at increasing magnification (left) and Raman spectra of fragment D (solid line) compared to several reference standards (pencil graphite, burnt carbon fibre and charcoal).

1000-1800cm^{-1} group			**2200-3400cm^{-1} group**	
Shift (cm^{-1})	**Shape**	**Notation**	**Shift (cm^{-1})**	**Shape**
1078 cm^{-1}	shoulder	D4	2710 cm^{-1}	very large band
1212 cm^{-1}	shoulder	D4'	2950 cm^{-1}	large band
1355 cm^{-1}	large intense band	D1	3178 cm^{-1}	large band
1504 cm^{-1}	added curve-fit form	D3		
1596 cm^{-1}	large intense band	G		
1705 cm^{-1}	shoulder	D_{1700}		

Tab. 2 Raman shift bands shown by the trapped dark particles in STM18-04 fragment D, with an occasional weak calcite peak residue at 1088 cm-1 (Fig.7). Notation from Deldicque et al. (2023).

3.2. Chronology

As there was not enough material, we did not attempt to date the black soot layers directly from the stalagmite, instead concentrating on dating the calcite above and below these layers.

Six U-series ages (2σ) were obtained on STM-18-04: they range from 15,139 ± 108 (18-04-03) to 13,170 ± 158 years (18-04-61) (uncorrected ages) (Table 3). Similar values of ^{238}U content were obtained for the samples (~224-293 ppb), except for one sample (18-04-104) for which it was significantly lower (~148 ppb). Measured $\delta^{234}U$ ($\delta^{234}U_M$) values ranged from 22.7 ± 1.5 ‰ (18-04-104) to 57.2 ± 1.6 ‰ (18-04-03).

There is a stratigraphic inversion at the top of the speleothem: the younger age was obtained for sample 18-04-61, taken more than 40 mm under 18-04-104 (14,101 ± 140 years) and 18-04-110 (14,790 ± 100 years). This can be explained by low $^{230}Th/^{232}Th$ ratios, 15.8 and 10.6 respectively, for the two uppermost samples, which attest that exogeneous thorium contamination is significant. Indeed, the lower the $^{230}Th/^{232}Th$ value, the highest is the contamination with detrital Th, i.e. which is not the product of ^{234}U. Ages were thus corrected, assuming an initial $^{230}Th/^{232}Th$ activity ratio of 1.5 ± 50%: corrected ages range from 14,437 ± 456 years for the base to 12,859 ± 1056 years for the top (Table 3). A second correction method, based on stratigraphic constraints, the STRUTages algorithm (Roy-Barman and Pons-Branchu, 2016), was used. Corrected values using this model did not significantly differ from those corrected using "*a priori*" values, with values ranging from 14,337 ± 218 (base) to 12,390 ± 544 years (top), but the STRUTages algorithm reduces the error range (Table 3). We used the STRUT ages for interpretation and discussion of the stalagmite.

Lab #	18-04 #	^{238}U (ppb)	^{232}Th (ppb)	$\delta^{234}U_M$ (‰)	($^{230}Th/^{238}U$)	($^{230}Th/^{232}Th$)	Age (years)	$\delta^{234}U_{initial}$ (‰)	Cor. age[†] (years)	STRUT age[‡] (years)
8559	3	223.54 ± 1.79	3.18 ± 0.03	57.2 ± 1.6	0.1370 ± 0.0007	30.0 ± 0.2	15,139 ± 108	59.6 ± 1.6	14,437 ± 456	14,337 ± 218
8561	7	249.61 ± 2.00	0.94 ± 0.01	55.4 ± 1.1	0.1303 ± 0.0005	108.1 ± 0.4	14,376 ± 75	57.6 ± 1.2	14,190 ± 168	14,161 ± 77
8562	12	292.78 ± 2.35	0.33 ± 0.01	54.3 ± 1.2	0.1284 ± 0.0004	358.6 ± 0.2	14,165 ± 67	56.6 ± 1.2	14,109 ± 95	14,094 ± 51
8635	61	283.49 ± 2.27	0.27 ± 0.01	40.4 ± 2.0	0.1183 ± 0.0011	374.4 ± 3.5	13,170 ± 158	41.9 ± 2.0	13,121 ± 183	13,111 ± 108
8563	104	147.61 ± 1.18	3.63 ± 0.03	22.7 ± 1.5	0.1239 ± 0.0010	15.8 ± 0.1	14,101 ± 140	23.6 ± 1.6	12,857 ± 757	12,661 ± 396
8564	110	238.18 ± 1.91	9.23 ± 0.07	34.4 ± 1.5	0.1311 ± 0.0006	10.6 ± 0.1	14,790 ± 100	35.7 ± 1.6	12,859 ± 1056	12,390 ± 544

Tab. 3. U-series data (2σ) obtained from PTS-STM 18-04. The second column refers to the sample number (see Fig. 2) and is the depth of the sample taken from the base of the speleothem (in mm). Ages (before 2020) were calculated using the following decay constants: $\lambda_{238} = 1.55125 \cdot 10^{10}$ (Jaffey et al., 1971), $\lambda_{234} = 2.82206 \cdot 10^{6}$, and $\lambda_{230} = 9.1705 \cdot 10^{6}$ (Cheng et al., 2013). $\delta^{234}U_M = ((^{234}U/^{238}U)_{measured}/(^{234}U/^{238}U)_{equilibrium} - 1) \times 1000$. $\delta^{234}U_{initial}$ was calculated based on ^{230}Th age (T): $\delta^{234}U_{initial} = \delta^{234}U_M \times e^{\lambda 234 \times T}$.

[†]Ages were corrected using a $^{230}Th/^{232}Th$ initial value of 1.5 ± 50%.

[‡]STRUT ages were corrected using stratigraphical constraints, assuming 30% of variability, resulting in a $(^{230}Th/^{232}Th)_0$ of 1.318 ± 0.213 (Roy-Barman and Pons-Branchu, 2016).

Lab Code	STM-18-04#	pMC	Age BP	Age cal BP	DCP (%)	- (%)	+ (%)
61118	03	18.86 ± 0.10	13,400 ± 45	16,298-15,975	11.9	0.9	1.6
61119	07	18.58 ± 0.11	13,520 ± 45	16,495-16,145	14.4	0.6	0.6
61120	12	18.87 ± 0.11	13,395 ± 45	16,293-15,967	13.6	0.4	1.2
61121	61	21.25 ± 0.10	12,440 ± 40	14,921-14,309	14.2	1.3	2.2
61122	104	23.42 ± 0.10	11,660 ± 35	13,530-13,455	12.5	6.2	1.3
61123	110	24.46 ± 0.11	11,315 ± 35	13,300-13,155	11.0	6.5	1.6

328 Tab. 4. ^{14}C results on calcite samples (as pMC: percent of Modern Carbon) and DCP (%). Ages were calibrated using Oxcal 4.4
329 (Bronk-Ramsey, 2001) and the IntCal20 curve (Reimer et al., 2020).

330

Lab Code	Sample Code	Square meter	Stratigraphic Unit	x	y	z	Age (BP)	Age (cal BP)
GifA13468/SacA37389	**PTS-Charb-1140**	G24	1	28	632	-153	12,360 ± 50	**14,840-14,139**
GifA15486/SacA44412	**PTS-Charb-1223**	E37	1	-188.2	1994.45	-309.3	12,160 ± 190	**14,930-13,608**
Lyon-19181/SacA-65113	**PTS-Charb-1521**	K25	2015-1	445	716	-158.5	12,040 ± 60	**14,053-13,795**
Lyon-19182/SacA-65114	**PTS-Charb-1525**	J25	A	385	731	-182	11,300 ± 50	**13,300-13,105**
Lyon-17823/SacA60975	**PTS-Charb-1548**	G22	1 (f.br.)	22	474	-142	12,850 ± 60	**15,574-15,164**

331 Tab. 5. ^{14}C results on charcoal samples from archaeological excavations at the entrance of the cave. Ages were calibrated using Oxcal
332 4.4 (Bronk-Ramsey, 2001) and the IntCal20 curve (Reimer et al., 2020).

These ages fall within MIS2 (29-14 ka, Lisiecki and Raymo, 2005) and are coeval with the Bølling-Allerød, 14.6-12.9 ka, and the Younger Dryas, 12.9-11.7 ka (Rasmussen et al., 2014) (Figure 8). More specifically, samples were taken immediately above and below the dark layers (respectively 18-04-03 and 07; 18-04-07 and 12; 18-04-104 and 110) to bracket the age of the fire events, and thus human presence in the cave. Modelled STRUT ages and their sampling depth within the stalagmite were combined to obtain an age-depth model using MOD-AGE (Hercman and Pawlak, 2012). Using the normal distribution of the U-series ages and depth measurements, modelled ages and depth within the stalagmite were obtained from Monte Carlo simulation (Figure 8). According to our data, the age of the oldest fire event, located at the bottom of the stalagmite, is between 14,337 ± 218 and 14,161 ± 77 years, and the second event between 14,161 ± 77 and 14,094 ± 51 years. The third and the fourth events, at the top of the speleothem, are dated to between 12,661 ± 396 and 12,390 ± 544 years.

The ^{14}C ages on calcite allowed us to estimate the dead carbon proportion (DCP, Table 4). They confirm the stability of the dead carbon input over time and the good stratigraphic coherence of the sequence. The DCP was calculated using U-Th ages as "true age", ^{14}C measurements, and atmospheric ^{14}C values from the IntCal20 calibration curve (Reimer et al. 2020) following Genty et al. (2001). DCP display low variation (from 11.9 +1.6 -0.9 % to 14.2 +2.2 -1.3 %). These values fall within the typical range of DCP values published for caves with thin soil (Genty et al., 2001; Griffiths et al., 2012; Noronha et al., 2014).

Four of the charcoals from nearby archaeological excavations yielded results between ca. 13,105 and 14,930 cal BP (Table 5). At 2σ, these results overlap with the period of growth of STM-18-04. In particular two of them (Charb-1140 and Charb-1223) could be related to the same fire event or, at least, one of the two earliest soot horizons at the base of STM-18-04 (Figure 8). This

would be consistent, at least for Charb-1223, whose stratigraphic position is similar to that of the two dark horizons at the base of STM-18-04.

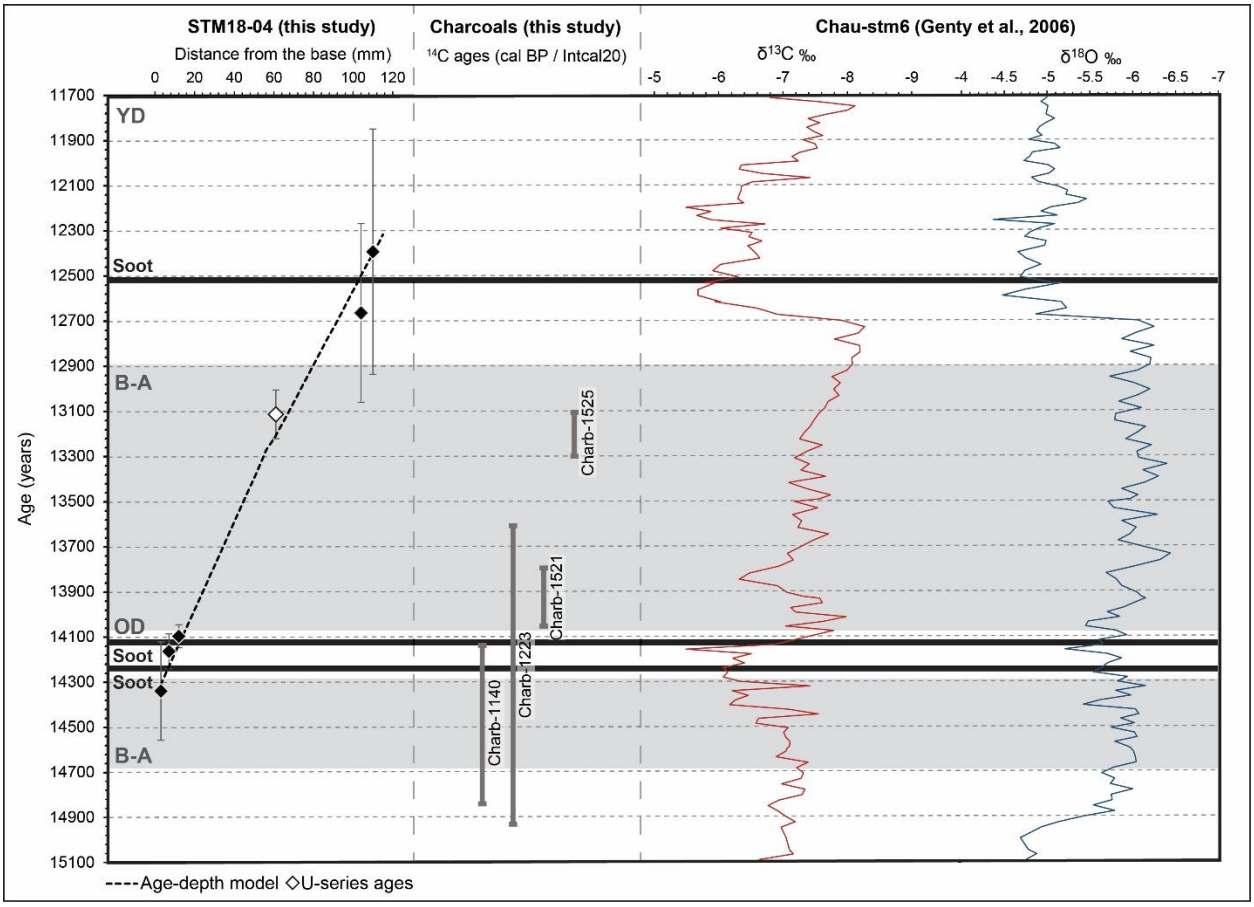

Figure 8. U-series (based on STRUT method) and ^{14}C age results and depth age model (MOD-AGE, dashed line) presented as a function of the $\delta^{13}C$ and $\delta^{18}O$ variations recorded in the Chau-stm6 stalagmite from the Chauvet Cave (data from Genty et al., 2006). The three plain black lines represent the approximate location of the soot layers identified in STM-18-04 and the black diamonds represent the U-series ages that bracket the soot layers. YD = Younger Dryas; B-A: Bølling-Allerød; OD = Older Dryas (ca. 14,150 years, see Figure 11 in Genty et al., 2006).

4. Discussion

By combining characterisation tools with dating techniques, we were able to characterise and to reconstruct the timing of human presence during the Tardiglacial era and the Termination I.

The hypothesis of an anthropogenic origin for the fire events recorded within STM-18-04 is corroborated by the radiocarbon results obtained on the charcoals collected nearby in association with lithic remains in archaeological layers at the cave entrance. The calibrated ages of at least three of these charcoals overlap the timespan of the first two fire events as bracketed by the calcite dating. Assuming that the fire events were related to anthropic activities, human presence at the cave entrance is thus attested during at least two phases, the first one between ca. 14,337 ± 218 and 14,094 ± 51 years, and the second one between 12,661 ± 396 and 12,390 ± 544 years.

The first phase identified falls within the Bølling-Allerød (ca. 14.6-12.9 ka, Rasmussen et al., 2014), and the second one within the Younger Dryas (ca. 12.9-11.7 ka, Rasmussen et al., 2014).

These periods of human activity at Points Cave are contemporary with the radiometric results obtained at several archaeological sequences in the Ardèche Gorge. While data are well documented at the regional scale for the Bølling-Allerød, contexts attributed to the Late Tardiglacial are often poorly preserved and/or dated. For example, the site of the Colombier II rock shelter shows evidence of human occupations dated between the Older Dryas and Allerød linked with fireplaces and remains of lithic or bone industry, attributed to the Upper Magdalenian and the Azilian (Onoratini, 1992; Joris, 2002; Bazile, 2014; Beauvais, 2022). The continuous sequence of this site shows similarities with other contemporary contexts such as Saut-du-Loup (Gilles, 1976), which demonstrate recurrent occupations during the Bølling-Allerød. In the Ardèche Gorge, several other sites lacking radiometric results also yielded lithic

390 remains attributed to the same technocomplexes, in particular the Baume d'Oulen (Beauvais et
391 al., 2020) as well as Baou-de-la-Sello and Huchard caves (Combier, 1967).
392 The results obtained at Points Cave thus fit well into the regional context of use of the central
393 part of the Ardèche River Gorge by human communities at the end of the Upper Palaeolithic
394 and/or beginnings of the Epipalaeolithic, possibly in connection with specialised hunting
395 activities (Lateur et al., 2019).
396 Our age results can be compared with those obtained on other speleothems for which
397 palaeoclimatic data are available. For instance, palaeoclimatic analyses of some of the Chauvet
398 Cave stalagmites (Genty et al., 2004), located upstream in the Ardèche gorges, enable
399 reconstructing the climatic conditions at the time of the human occupation of Points Cave, since
400 they precipitated during the same period. In particular, it is possible to match the ages obtained
401 from STM-18-04 with Chau-stm6, dated between ca. 11,498-32,872 years (Genty et al., 2006)
402 (Figure 8). $\delta^{13}C$ and $\delta^{18}O$ analyses of this stalagmite give some insights into the regional
403 paleoclimatic record during the last deglaciation. In speleothems, an increase in both $\delta^{13}C$ and
404 $\delta^{18}O$ values is interpreted as a cold event: the reduction of vegetation and soil activity due to a
405 decrease in temperature leads to an increase in $\delta^{13}C$ during cold periods; in turn, an increase in
406 $\delta^{18}O$ values reflects a decrease in temperature. The palaeoclimatic record of Chau-stm6 shows
407 three peaks in less negative values of $\delta^{13}C$ and $\delta^{18}O$: at ca. 14,150 years, 12,590 years, and
408 12,200 years (Figure 8), indicating climate degradation for these intervals. A paleoclimatic
409 record at Salamandre cave (Cèze Valley, a few kilometers away from Points Cave) confirms that
410 the Younger Dryas in the region is marked by the degradation of soil activity (Drugat et al.,
411 2019). Interestingly, our U-series ages, which bracket the fire events between 14,337 ± 218 and
412 14,094 ± 51 years and 12,661 ± 396 and 12,390 ± 544 years, match with two of these three

events of cold climate, ca. 14,150 years and 12,590 years. Moreover, the cold event observed at a maximum amplitude ca. 14,150 years, recorded within the Bølling-Allerød, is synchronous with the Older Dryas, ca. 14.1 ka (Hughen, et al., 2000) (see discussion in Genty et al., 2006; Genty, 2012). We can thus conclude that the humans who produced the fires at Points Cave likely visited the cave during cold events (but sufficiently humid to allow speleothem growth), possibly the Older Dryas, and during the Younger Dryas.

5. Conclusions

The study of the stalagmite STM-18-04 showed that proxies such as speleothems are a significant source of information when reconstructing human occupation phases at a cave site. The combination of microscopy and spectroscopy analyses (optical microscopy, SEM, µRaman, and FTIR spectroscopy) proved to be a valuable toolset to reveal the presence of soot, which can be attributed to fire events within the cave during human occupation. At Points Cave, the analyse of STM-18-04 thus gave new insights into the human activities that took place at the entrance of the cave during the Upper Palaeolithic. Thanks to the characterisation of the soot layers and the dating of its calcite matrix, we showed that the cave was visited several times during the Upper Magdalenian and/or beginning of the Epipalaeolithic, respectively between around 14,200-14,100 and 12,500 years, in agreement with ^{14}C dating of charcoals recovered during the excavations. The comparison of our data with published regional palaeoclimatic records (Drugat et al., 2019; Genty et al., 2006) made it possible to assign these fire events, and thus human presence, to cold phases, likely the Older and Younger Dryas.

Ultimately, all of this contributes to refining the overall timing, palaeoclimatic context, and recurrence times of human activities at Points Cave, during the Upper Palaeolithic. However,

436 the relationship between the entrance of the cave, where the fire activities took place, and the
437 cave art, located in the depths of the cave, still needs to be investigated.
438
439 **Acknowledgments**
440 This work was supported by the DRAC Occitanie (French Ministry of Culture) and by the
441 French National Research Agency (ANR-18-CE27-0004 ApART). We would like to thank
442 Robin Furestier, Charlène Girard, and Léo Lacheray (FARPA) for managing the funding, and the
443 municipality of Saint-Martin-d'Ardèche (site owner) for allowing us to carry out research in the
444 cave. Our thanks also go to Patricia Guillermin, Philippe Barth, Françoise Prud'Homme, and
445 Sonia Stocchetti (Aven d'Orgnac – Cité de la Préhistoire) for providing accommodation and
446 technical support. A special thank you to Isabelle Couchoud for providing material resources
447 during sampling at EDYTEM laboratory. Michael Toffolo was supported by a grant from IdEx
448 Bordeaux (ANR-10-IDEX-03-02). We thank Yannick Lefrais for assistance during SEM
449 analysis at Archéosciences Bordeaux, Carlos Sáiz (CENIEH) for preparing the thin section of the
450 speleothem, the PANOPLY platform (Plateforme Analytique Géosciences Paris Saclay) for the
451 use of the MC-ICPMS and the Centre de Datation par le Radiocarbone (CDRC) in Lyon
452 (France).
453
454 **References**
455 Ambert P., Guendon J.-L., Galant P., Quinif Y., Gruneisen A., Colomer A., Dainat D., Beaumes
456 B., Requirand C., 2005. Attribution des gravures paléolithiques de la grotte d'Aldène
457 (Cesseras, Hérault) à l'Aurignacien par la datation des remplissages géologiques. C. R.
458 Palevol, n°4, pp. 275-284.

Aubert, M., Brumm, A., Ramli, M., Sutikna, T., Saptomo, E. W., Hakim, B., Morwood M. J., van den Bergh G. D., Dosseto, A., 2014. Pleistocene cave art from Sulawesi, Indonesia, Nature, 514(7521), 223-227.

Azéma M., Gély B., Bourrillon R., Galant P., 2012. L'art paléolithique de la Baume Latrone (France, Gard) : Nouveaux éléments de datation. INORA, n°64, pp. 6-12.

Baffier D., Feruglio V., 1998. Premières observations sur deux nappes de ponctuations de la Grotte Chauvet (Vallon-Pont-d'Arc, Ardèche, France). INORA, n°21, pp. 1-2.

Bazile F., 2014. Le bassin méditerranéen du Rhône : Un carrefour de traditions culturelles au Tardiglaciaire. Vauvert, Centre de recherches et de documentation du Gard (Études quaternaires languedociennes, Mémoire, 2), 160 p.

Beauvais P.-A., 2022. Les subdivisions du tardiglaciaire rhodanien à l'épreuve de l'analyse relationnelle des industries lithiques, Thèse de Doctorat, Université Toulouse Jean-Jaurès, 407 p.

Beauvais P.-A., Guillermin P., Teyssandier N., 2020. Nouvelles données sur un ensemble lithique du Magdalénien supérieur des gorges de l'Ardèche : La grotte de la Baume d'Oulen, Labastide-de-Virac, Le Garn (Ardèche, Gard). Société préhistorique française, 2020, Séances de la Société préhistorique française, pp. 295-317.

Boccaccio, G., 2018. Résultats préliminaires de l'étude de la série lithique de la grotte aux Points: typologie et technologie. Karstologia n°72, 37-44.

Bourdin, C., Douville, E., Genty, D., 2011. Alkaline-earth metal and rare-earth element incorporation control by ionic radius and growth rate on a stalagmite from the Chauvet cave, Southeastern France. Chemical Geology 290, 1-11.

Bronk Ramsey, C., 2001. Development of the radiocarbon calibration program OxCal. Radiocarbon, 43(2A), 355–363.

Brunel, E., Chailloux, D., Chauvet, J., Dugas, A., Hillaire, C., Raimbault, M., Renda, M., Terres, S., 2008. La grotte aux Points (commune d'Aiguèze, Gard). Ardèche Archéologie 28, 23-28.

Brunel, E., Chauvet, J.M., Hillaire, C., 2018. La grotte aux Points d'Aiguèze: récits de découverte d'une ornementation pariétale. Karstologia, 13-14.

Chauvet J.-M., Brunel Deschamps E., Hillaire C., 1995. *La Grotte Chauvet à Vallon-Pont-d'Arc*. Paris, Seuil.

Cheng, H., Lawrence Edwards, R., Shen, C.-C., Polyak, V.J., Asmerom, Y., Woodhead, J., Hellstrom, J., Wang, Y., Kong, X., Spötl, C., Wang, X., Calvin Alexander, E., 2013. Improvements in ^{230}Th dating, ^{230}Th and ^{234}U half-life values, and U–Th isotopic measurements by multi-collector inductively coupled plasma mass spectrometry. Earth and Planetary Science Letters 371-372, 82-91.

Clottes J., Chauvet J.-M., Brunel-Deschamps É., Hillaire Ch., Daugas J.-P., Arnold M., Cachier H., Évin J., Fortin Ph., Oberlin Ch., Tisnerat N. Valladas H., 1995. Les Peintures paléolithiques de la Grotte Chauvet-Pont d'Arc (Ardèche, France) : datations directes et indirectes par la méthode du radiocarbone. C.R. de l'Académie des Sciences de Paris, n°320, série IIa, pp. 1133-1140.

Combier J., 1967. Le Paléolithique de l'Ardèche dans son cadre paléoclimatique, Bordeaux, Imprimerie Delmas (Publications de l'Institut de Préhistoire de l'université de Bordeaux, Mémoire, 4), 462 p.

503 Cuzange, M.-T., Delqu-Kolic, E., slar, T., Grootes, P.M., Higham, T., Kaltnecker, E., Nadeau,
504 M.-J., erlin, C., Paterne, M., va, J., Bron, C., Valladas, H., tes, J., Geneste, J.-M., 2007.
505 Radiocarbon Intercomparison Program for Chauvet cave, Radiocarbon 49, 339-347.
506 Drugat, L., Pons-Branchu, E., Douville, E., Foliot, L., Bordier, L., Roy-Barman, M., 2019. Rare
507 earth and alkali elements in stalagmites, as markers of Mediterranean environmental
508 changes during Termination I, Chemical Geology 525, 414-423.
509 Deldicque D., Rouzaud J.-N., Vandevelde S., Medina-Alcaide M.A., Ferrier C., Perrenoud C.,
510 Pozzi J.-P., Cabanis M., 2023, Effects of oxidative weathering on Raman spectra of
511 charcoal and bone chars: consequences in archaeology and paleothermometry. Comptes
512 Rendus. Géoscience, 355 (G1), 1-22.
513 Dumoulin, J.P., Comby-Zerbino, C., Delqué-Količ, E., Moreau, C., Caffy, I., Hain, S., Perron,
514 M., Thellier, B., Setti, V., Berthier, B., Beck, L., 2017. Status Report on Sample
515 Preparation Protocols Developed at the LMC14 Laboratory, Saclay, France: From Sample
516 Collection to 14C AMS Measurement, Radiocarbon 59, 713-726.
517 Farmer, V.C., 1974. The Infrared Spectra of Minerals. Mineralogical Society, London.
518 Gély B., 2005. La Grotte Chauvet à Vallon-Pont-d'Arc (Ardèche) : Le contexte régional
519 paléolithique. In : Geneste J.-M.(dir.) Recherches pluridisciplinaires dans la Grotte
520 Chauvet – Journées SPF, Lyon, 11-12 octobre 2003. Bulletin de la Société Préhistorique
521 Française, n°102(1), pp. 17-33.
522 Genty, D., Dauphin, Y., Deflandre, G., Quinif, Y., 1997. Exemples de particules d'origine
523 anthropique piégées dans les lamines de croissance de stalagmites - Intérêt pour la
524 reconstitution des environnements humains anciens, Quaternaire 8, 149-157.

525 Genty, D., Baker, A., Massault, M., Proctor, C., Gilmour, M., Pons-Branchu, E., Hamelin, B.,
526 2001. Dead carbon in stalagmites: carbonate bedrock paleodissolution vs. ageing of soil
527 organic matter. Implications for ^{13}C variations in speleothems, Geochimica et
528 Cosmochimica Acta 65, 3443-3457.
529 Genty D., Ghaleb B., Plagnes V., Causse C., Valladas H., Blamart D., Massault M., Geneste J.-
530 M., Clottes J., 2004. Datations U/Th (TIMS) et ^{14}C (AMS) des stalagmites de la grotte
531 Chauvet (Ardèche, France) : intérêt pour la chronologie des événements naturels et
532 anthropiques de la grotte. C. R. Palevol, n°3, pp. 629-42.
533 Genty, D., Blamart, D., Ghaleb, B., Plagnes, V., Causse, C., Bakalowicz, M., Zouari, K., Chkir,
534 N., Hellstrom, J., Wainer, K., Bourges, F., 2006. Timing and dynamics of the last
535 deglaciation from European and North African δ13C stalagmite profiles—comparison with
536 Chinese and South Hemisphere stalagmites, Quaternary Science Reviews 25, 2118-2142.
537 Genty, D., 2012. Les spéléothèmes de la grotte Chauvet-Pont-d'Arc : apports chronologiques et
538 paléoclimatiques. Synthèse des travaux publiés, Collection EDYTEM. Cahiers de
539 géographie, 79-88.
540 Genuite K., Voinchet P., Delannoy J.-J., Bahain J.-J., Monney J., Arnaud J., Bruxelles L.,
541 Moncel M.-H., Philippe A., Pons-Branchu E., Revil A., Richard M., Jaillet S., 2022.
542 Middle and Late Pleistocene evolution of the Ardèche river archaeological landscapes
543 (France). *Quaternary Science Review*, 297, 107812.
544 Gilles R., 1976. L'abri du Saut-du-Loup. *In* Combier J., Thévenot P. (éds.), Livret-guide de
545 l'excursion A8 : Bassin du Rhône au Paléolithique et Néolithique. IX^{ème} congrès UISPP,
546 13-18 septembre 1976, Nice. p. 206.

Griffiths, M.L., Fohlmeister, J., Drysdale, R.N., Hua, Q., Johnson, K.R., Hellstrom, J.C., Gagan, M.K., Zhao, J.X., 2012. Hydrological control of the dead carbon fraction in a Holocene tropical speleothem. Quaternary Geochronology 14, 81–93.

Guibert P., Brodard A., Quiles A., Geneste J. M., Baffier D., Debard E., Ferrier C., 2015**.** When were the walls of the Chauvet-Pont d'Arc Cave heated? A chronological approach by thermoluminescence. Quaternary Geochronology, n°29, pp. 36-47.

Hellstrom, J., 2006. U–Th dating of speleothems with high initial 230Th using stratigraphical constraint. Quaternary Geochronology 1, 289-295.

Hercman, H., Pawlak, J., 2012. MOD-AGE: An age-depth model construction algorithm. Quaternary Geochronology 12, 1-10.

Hoffmann, D.L., Pike, A.W.G., García-Diez, M., Pettitt, P. B., Zilhão, J., 2016. Methods for U-series dating of $CaCO_3$ crusts associated with Palaeolithic cave art and application to Iberian sites, Quaternary Geochronology 36, 104-119.

Hughen, K.A., Southon, J.R., Lehman, S.J., Overpeck, J.T., 2000. Synchronous Radiocarbon and Climate Shifts During the Last Deglaciation, Science 290, 1951-1954.

Ivanovich, M., Harmon, R.S., 1992. Uranium-Series Disequilibrium: Applications to Earth, Marine, and Environmental Sciences (2nd edition). Clarendon Press, Oxford, 910 p.

Jaffey, A.H., Flynn, K.F., Glendenin, L.E., Bentley, W.C., Essling, A.M., 1971. Precision Measurement of Half-Lives and Specific Activities of ^{235}U and ^{238}U. Physical Review C 4, 1889-1906.

Joris C., 2002. Les industries magdaléniennes de l'Ardèche dans le contexte du Bassin méditerranéen, Montagnac, Ed. M. Mergoil (Préhistoires), 154 p.

570 Lafon-Pham, D., Konik, S., Monney, J., 2022. On-site spectroradiometric analysis of Palaeolithic
571 cave art: Investigating colour variability in the red rock art of Points cave (France), Journal
572 of Archaeological Science: Reports 42, 103384.
573 Lateur, N., Fourvel, J. B., Jeannet, M., Philippe, M., 2019. Comportements de subsistance
574 paléolithiques et relations entre l'Homme et les Carnivores à la grotte aux Points (Aiguèze,
575 Gard) au travers de l'archéozoologique et taphonomique des restes fauniques. *Karstologia*,
576 *73*, 13-24.
577 Lisiecki, L.E., Raymo, M.E., 2005. A Pliocene-Pleistocene stack of 57 globally distributed
578 benthic δ18O records. Paleoceanography 20, PA1003.
579 Monney J., Combier J., Kaltnecker E., Lateur N., Moreau C., Stocchetti S., Valladas H., 2014.
580 Nouveaux éléments de discussion chronologiques dans le paysage des Grottes ornées de
581 l'Ardèche : Oulen, Chabot et Tête-du-Lion. In : Paillet P.(dir.) Les arts de la Préhistoire :
582 micro-analyses, mises en contextes et conservation. Actes du colloques MADAPCA, 16-18
583 novembre 2011, Paris. Paléo, n° spécial 2014, p. 271-284.
584 Monney J., Jaillet S.. 2019. Fréquentations humaines, Ornementation pariétale et processus
585 naturels: Mise en place d'un cadre chronologique pour la grotte aux Points d'Aiguèze.
586 Karstologia, n°73, p. 49-62.
587 Monney, J., 2018a. La Grotte aux Points d'Aiguèze, petite sœur de la grotte Chauvet, et les
588 recherches menées dans le cadre du projet "Datation Grottes Ornées". Karstologia 72, 1-12.
589 Monney, J., 2018b. L'art pariétal paléolithique de la grotte aux Points d'Aiguèze: définition d'un
590 dispositif pariétal singulier et discussion de ses implications, Karstologia, 45-60.
591 Mook, W.G., van der Plicht, J., 1999. Reporting ^{14}C Activities and Concentrations, Radiocarbon
592 41, 227-239.

593 Moreau, C., Caffy, I., Comby, C., Delqué-Količ, E., Dumoulin, J.P., Hain, S., Quiles, A., Setti,
594 V., Souprayen, C., Thellier, B., Vincent, J., 2013. Research and Development of the
595 Artemis 14C AMS Facility: Status Report, Radiocarbon 55, 331-337.
596 Moreau, C., Messager, C., Berthier, B., Hain, S., Thellier, B., Dumoulin, J.-P., Caffy, I., Sieudat,
597 M., Delqué-Količ, E., Mussard, S., Perron, M., Setti, V., Beck, L., 2020. Artemis, the 14C
598 ams facility of the LMC14 national laboratory: a status report on quality control and
599 microsample procedures, Radiocarbon 62, 1755-1770.
600 Noronha, A.L., Johnson, K.R., Hu, C., Ruan, J., Southon, J.R., Ferguson, J.E., 2014. Assessing
601 influences on speleothem dead carbon variability over the Holocene: implications for
602 speleothem-based radiocarbon calibration. Earth and Planetary Science Letters 394, 20–29.
603 Onoratini, G., Combier, J., Ayroles, P., 1992. Datation ^{14}C d'une gravure pariétale de bouquetin
604 de l'abri magdalénien du Colombier (Vallon-Pont-d'Arc, Ardèche). *Comptes rendus de*
605 *l'Académie des sciences. Série 2, Mécanique, Physique, Chimie, Sciences de l'univers,*
606 *Sciences de la Terre*, *314*(4), 405-410.
607 Pike, A. W., Hoffmann, D. L., García-Diez, M., Pettitt, P. B., Alcolea, J., De Balbin, R.,
608 González-Sainz C., de las Heras C., Lasheras J. A., Montes R., Zilhão, J., 2012. U-Series
609 Dating of Paleolithic Art in 11 Caves in Spain, Science 336, 1409-1413.
610 Poduska, K.M., Regev, L., Boaretto, E., Addadi, L., Weiner, S., Kronik, L., Curtarolo, S., 2011.
611 Decoupling Local Disorder and Optical Effects in Infrared Spectra: Differentiating
612 Between Calcites with Different Origins. Advanced Materials 23, 550-554.
613 Pons-Branchu, E., Bourrillon, R., Conkey, M. W., Fontugne, M., Fritz, C., Gárate, D., Quiles A.,
614 Rivero O., Sauvet G., Tosello G., Valladas H., White, R., 2014a. Uranium-series dating of

carbonate formations overlying Paleolithic art: interest and limitations, Bulletin de la Société préhistorique française, 111(2), 211-224.

Pons-Branchu, E., Douville, E., Roy-Barman, M., Dumont, E., Branchu, P., Thil, F., Frank, N., Bordier, L., Borst, W., 2014b. A geochemical perspective on Parisian urban history based on U–Th dating, laminae counting and yttrium and REE concentrations of recent carbonates in underground aqueducts. Quaternary Geochronology 24, 44-53.

Pons-Branchu E., Barbarand J., Caffy I. Dapoigny A., Drugat L., Dumoulin J.P., Medina Alcaide M.A., Nouet J., Sanchidrián Torti J.L., Tisnerat-Laborde N., Jiménez de Cisneros, Valladas H., 2022. U-series and radiocarbon cross dating of speleothems from Nerja Cave (Spain): evidence of open system behavior. Implication for the Spanish rock Art chronology. Quaternary Sciences Review 290, 107634.

Quiles, A., Valladas, H., Bocherens, H., Delqué-Količ, E., Kaltnecker, E., van der Plicht, J., Delannoy, J.-J., Feruglio, V., Fritz, C., Monney, J., Philippe, M., Tosello, G., Clottes, J., Geneste, J.-M., 2016. A high-precision chronological model for the decorated Upper Paleolithic cave of Chauvet-Pont d'Arc, Ardèche, France, Proceedings of the National Academy of Sciences 113, 4670-4675.

Quiles, A., Valladas, H., Geneste, J.M., Clottes, J., Baffier, D., Berthier, B., Brock, F., Bronk Ramsey, C., Delqué-Količ, E., Dumoulin, J.P., Hajdas, I., Hippe, K., Hodgins, G.W.L., Hogg, A., Jull, A.J.T., Kaltnecker, E., de Martino, M., Oberlin, C., Petchey, F., Steier, P., Synal, H.A., van der Plicht, J., Wild, E.M., Zazzo, A., 2013. Second Radiocarbon Intercomparison Program for the Chauvet-Pont d'Arc Cave, Ardèche, France, Radiocarbon 56, 883-850.

637 Rasmussen, S.O., Bigler, M., Blockley, S.P., Blunier, T., Buchardt, S.L., Clausen, H.B.,
638 Cvijanovic, I., Dahl-Jensen, D., Johnsen, S.J., Fischer, H., Gkinis, V., Guillevic, M., Hoek,
639 W.Z., Lowe, J.J., Pedro, J.B., Popp, T., Seierstad, I.K., Steffensen, J.P., Svensson, A.M.,
640 Vallelonga, P., Vinther, B.M., Walker, M.J.C., Wheatley, J.J., Winstrup, M., 2014. A
641 stratigraphic framework for abrupt climatic changes during the Last Glacial period based
642 on three synchronized Greenland ice-core records: refining and extending the INTIMATE
643 event stratigraphy. Quaternary Science Reviews 106, 14-28.
644 Regev, L., Poduska, K.M., Addadi, L., Weiner, S., Boaretto, E., 2010. Distinguishing between
645 calcites formed by different mechanisms using infrared spectrometry: archaeological
646 applications. Journal of Archaeological Science 37, 3022-3029.
647 Reimer, P.J., Austin, W.E.N., Bard, E., Bayliss, A., Blackwell, P.G., Bronk Ramsey, C., Butzin,
648 M., Cheng, H., Edwards, R.L., Friedrich, M., Grootes, P.M., Guilderson, T.P., Hajdas, I.,
649 Heaton, T.J., Hogg, A.G., Hughen, K.A., Kromer, B., Manning, S.W., Muscheler, R.,
650 Palmer, J.G., Pearson, C., van der Plicht, J., Reimer, R.W., Richards, D.A., Scott, E.M.,
651 Southon, J.R., Turney, C.S.M., Wacker, L., Adolphi, F., Büntgen, U., Capano, M., Fahrni,
652 S.M., Fogtmann-Schulz, A., Friedrich, R., Köhler, P., Kudsk, S., Miyake, F., Olsen, J.,
653 Reinig, F., Sakamoto, M., Sookdeo, A., Talamo, S., 2020. The IntCal20 Northern
654 Hemisphere Radiocarbon Age Calibration Curve (0–55 cal kBP), Radiocarbon 62, 725-
655 757.
656 Richards, D.A., Dorale, J.A., 2003. Uranium-series chronology and environmental applications
657 of speleothems, in: Bourdon, B., Henderson, G.M., Lundstrom, C.C., Turner, S.P. (Eds.),
658 Uranium-series geochemistry. Reviews in Mineralogy & Geochemistry, pp. 407-460.

Rouzaud, F., 1978. La Paléospéléologie : L'Homme et le milieu souterrain pyrénéen au Paléolithique supérieur. Toulouse : Archives d'Ecologie Préhistorique.

Roy-Barman, M., Pons-Branchu, E., 2016. Improved U–Th dating of carbonates with high initial 230Th using stratigraphical and coevality constraints. Quaternary Geochronology 32, 29-39.

Sadier B., Delannoy J.-J., Benedetti L., Bourles D., Jaillet S., Geneste J.-M., Lebatard A.-M., Arnold M., 2012. Further constraints on Chauvet cave artwork elaboration, Proceedings of the National Academy of Sciences, n°109(21), pp. 8002-8006.

Theurer T., Muirhead D.K., Jolley D., Mauquoy D., 2021, The applicability of Raman spectroscopy in the assessment of palaeowildfire intensity. Palaeogeography Palaeoclimatology Palaeoecology, 570, 110363.

Valladas, H., Clottes, J., Geneste, J.M., Garcia, M.A., Arnold, M., Cachier, H., Tisnerat-Laborde, N., 2001. Palaeolithic paintings: Evolution of prehistoric cave art. Nature 413, 479-479.

Valladas H., Quiles A, Delque-Kolic M., Kaltnecker E., Moreau C., Pons Branchu E., Vanrel L, Olive M., Delestres X (2017). Radiocarbon dating of the decorated Cosquer cave (France). Radiocarbon, 59 (2) 621-633.

Van der Marel, H.W., Beutelspacher, H., 1976. Atlas of Infrared Spectroscopy of Clay Minerals and their Admixtures. Elsevier Scientific Publishing Company, Amsterdam.

Vandevelde, S., Brochier, J.É., Petit, C., Slimak, L., 2017. Establishment of occupation chronicles in Grotte Mandrin using sooted concretions: Rethinking the Middle to Upper Paleolithic transition, Journal of Human Evolution 112, 70-78.

Xu, B., Toffolo, M.B., Regev, L., Boaretto, E., Poduska, K.M., 2015. Structural differences in archaeologically relevant calcite. Analytical Methods 7, 9304-9309.

Supplementary online material (SOM)

STM18-04

	Center			Area			Height				Halfwidth		Shape	
Peak ID	Shift (cm^{-1})	*Err.*		(cts)	(%)	(cts)	*Err.*	Rel. (%)	*Err (%)*	(cm^{-1})	Err.	%Lorz.	Err.
1	1077.5	*		1003765	6.6	8599	*44*	5.7	*0.5*	109.7	0.6	0.00	*
2	1087.6	*		68578	0.5	8694	*113*	5.7	*1.3*	6.4	0.1	0.34	*
3	1211.3	*0.2*		4450359	29.4	31195	*140*	20.6	*0.5*	134.0	0.2	0.00	*
4	1356.0	*		22872960	151.2	120916	*39*	79.9	*<0.1*	171.0	0.3	0.11	<0.01
5	1503.9	*0.1*		3762738	24.9	34831	*103*	23.0	*0.3*	101.5	0.3	0.00	*
6	1597.0	*		15122838	100.0	151352	*61*	100.0	*<0.1*	83.2	0.0	0.32	<0.01
7	1703.0	*		658751	4.4	10880	*58*	7.2	*0.5*	56.9	0.3	0.00	*
8	2698.3	*2.0*		12923965	85.5	33096	*181*	21.9	*0.6*	366.9	2.6	0.00	*
9	2943.4	*0.9*		6994966	46.3	27495	*425*	18.2	*1.5*	239.0	3.2	0.00	*
10	3175.0	*1.9*		2873275	19.0	13097	*160*	8.7	*1.2*	206.1	2.6	0.00	*

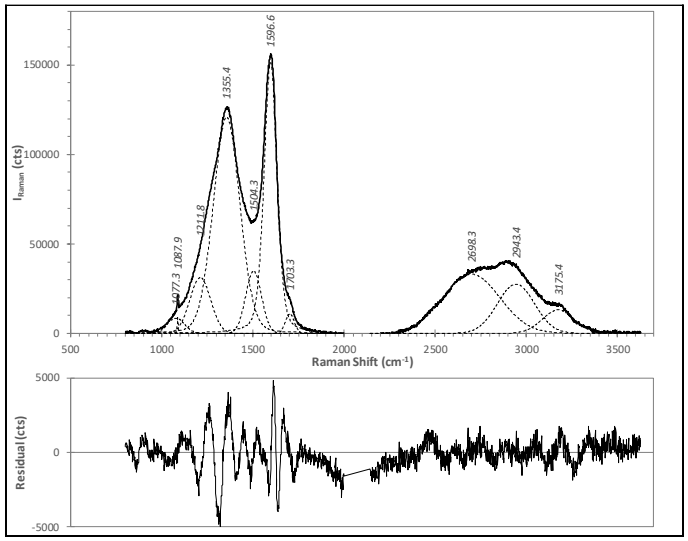

PBC (Pine Burned Charcoal)

	Center			Area		Height				Width		Shape	
Peak ID	Shift (cm^{-1})	*Err.*		(cts)	Rel. (%)	(cts)	*Err.*	Rel. (%)	*Err (%)*	(cm^{-1})	Err.	%Lorz.	Err
1	1077.5	*		3077136	32.0	13306	*303*	14.4	*2.3*	175.3	1.3	0.83	0.03
2	1087.6												
3	1224.7	*1.8*		5133637	53.3	30817	*789*	33.4	*2.6*	156.5	1.6	0.00	0.06
4	1356.0	*		12854727	133.5	79791	*763*	86.5	*1.0*	151.3	2.3	0.00	0.02
5	1498.8	*0.7*		5496466	57.1	40297	*687*	43.7	*1.7*	128.1	3.1	0.00	*
6	1592.6	*0.2*		9629756	100.0	92280	*695*	100.0	*0.8*	89.6	0.2	0.24	0.01
7	1703.0	*		704219	7.3	9193	*114*	10.0	*1.2*	72.0	0.8	0.00	*
8	2682.8	*3.0*		9994655	103.8	17679	*105*	19.2	*0.6*	535.9	3.5	0.00	*
9	2951.2	*1.4*		1818503	18.9	5862	*255*	6.4	*4.4*	291.4	6.6	0.00	*
10	3177.5	*1.3*		197192	2.0	2088	*64*	2.3	*3.1*	88.7	3.3	0.00	*

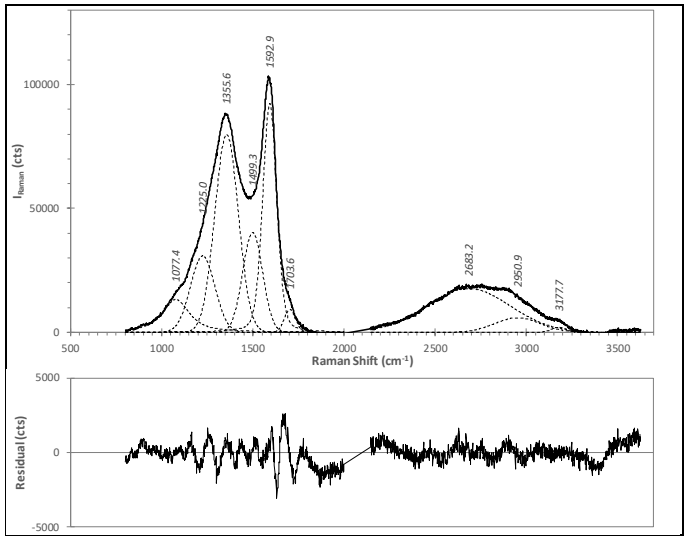

Tab. S1. Curve fitting results for STM18-04 black included matter and PBC burned charcoal reference shown in figure 7. Relative areas and heights by reference to 1592-1597cm^{-1} peak id 6. * Fixed shift and/or shape.